Teraherz Pulse Near-Field Microscopes

Article · October 2012

DOI: 10.1007/978-94-007-3965-9_13

4 authors, including:

Kiwon Moon
Electronics and Telecommunications Resear…
45 PUBLICATIONS **184** CITATIONS
SEE PROFILE

Youngwoong Do
Pohang University of Science and Technology
12 PUBLICATIONS **65** CITATIONS
SEE PROFILE

Haewook Han
Pohang University of Science and Technology
43 PUBLICATIONS **291** CITATIONS
SEE PROFILE

Terahertz Near-Field Microscope: Analysis and Measurements of Scattering Signals

Kiwon Moon, Euna Jung, Meehyun Lim, Youngwoong Do, and Haewook Han, *Member, IEEE*

(Invited Paper)

***Abstract*—We present the analysis and measurements of scattering signals of a terahertz pulse scattering-type near-field microscope. We used a self-consistent line dipole image method for the quantitative analysis of the THz near-field interaction. The line scan across a gold film demonstrated that the terahertz miscroscope has a nanoscale resolution of ∼80 nm. The measurements of scattering signals on gold and silicon substrates were in good agreement with calculations.**

***Index Terms*—Terahertz time-domain spectroscopy, terahertz scanning near-field microscope, terahertz wave.**

I. Introduction

NANOSCALE near-field imaging in the terahertz (THz) spectral range provides a powerful means for studying intriguing phenomena such as intermolecular vibrational spectroscopy and dynamic charge transport in a variety of quantum-confined nanostructures. Conventional THz time-domain spectroscopy (TDS) can provide macroscopic imaging averaged over an ensemble of such nanostructures, which inevitably suffers from inhomogeneous spectral broadening. Moreover, its spatial resolution is limited to $\sim\lambda/2$ by diffraction. Therefore, several types of THz pulse scanning near-field optical microscopes (SNOMs) have been developed to achieve sub-wavelength resolutions [1]–[9].

In contrast to visible or IR SNOMs, most THz SNOMs have been based on THz pulse TDS systems [1]–[8], making it possible to perform broadband coherent THz spectroscopy. Among the THz SNOM systems, the scattering-type SNOM (s-SNOM) has been the most successful technique so far in terms of spatial resolution and image quality [6]–[13]. In the THz s-SNOM, the scattered field from the tip apex is measured in the far-field region. Sub-micrometer resolutions are enabled by the strongly localized near-field around the probe tip [14]. Thus, it is essential to understand the near-field interaction in the tip-substrate system, and there have been several analytic models [15]–[18] and also numerical simulations [19], [20] to solve the problems. The most popular approach has been the point dipole image method (PDIM) [8]–[12] where the probe tip is replaced by a polarizable point dipole [10]. The PDIM has been widely used to analyze experimental data [8]–[12], and has provided qualitative understanding on s-SNOMs, including resolution [10] and optical phase contrast [11]. However, because the electromagnetic boundary conditions are not fully matched on the surface of the probe sphere, the PDIM becomes incorrect as the probe sphere approaches the substrate [15]–[18].

In this work, we analyze the THz scattering signals of a THz pulse s-SNOM by using a self-consistent line dipole image method (LDIM) [21]–[23]. We also present a line scan across the edge of a gold film on a GaAs substrate, showing that the THz s-SNOM has a nanoscale resolution of ∼80 nm. The measurements of the THz scattering signals on gold and GaAs surfaces were in reasonably good agreement with the LDIM calculations.

II. Instrumentations

The THz s-SNOM system was based on a THz TDS system combined with an atomic force microscope (AFM). The THz TDS system generates the THz pulses incident on the probe tip and detects the THz scattering signals. The sample scanning and the distance between the s-SMOM and the sample surface were precisely controlled by the AFM.

A. THz TDS System

Sub-picosecond THz pulses were generated from an InAs substrate pumped by a femtosecond laser, and measured by a photoconductive antenna on a low-temperature-grown (LTG) GaAs substrate using optical gate detection techniques [24]–[26]. This optical gating detection makes it possible to directly measure the transient electric fields of the THz pulses, providing both amplitude and phase spectra, whereas the conventional THz frequency-domain spectroscopy can usually measure only the amplitude spectrum.

B. AFM System and Background Suppression

The first nanoscale THz near-field imaging was based on a scanning tunneling microscope (STM) where the tunneling current was used to control the probe-substrate gap distance [5]. Although the STM can provide the highest spatial resolution among the scanning probe microscopes (SPMs), the principal disadvantage is that the tunneling current always requires a conducting substrate. Since many materials used in THz s-SNOMs are not conducting, we used the AFM which can operate on both

Manuscript received April 09, 2011; revised June 06, 2011; accepted June 06, 2011. Date of current version August 31, 2011. This work was supported in part by the National Research Laboratory Program (R0A-2005-001-10252-0), in part by the Basic Science Research Program (2009-0083512), and in part by the Priority Research Centers Program through the National Research Foundation of Korea (NRF) funded by the Ministry of Education, Science and Technology (2010-0029711) and by the Brain Korea 21 Project in 2011.

The authors are with the Department of Electrical Engineering, POSTECH, Pohang 790-784, Korea (e-mail: hhan@.postech.ac.kr).

Digital Object Identifier 10.1109/TTHZ.2011.2159876

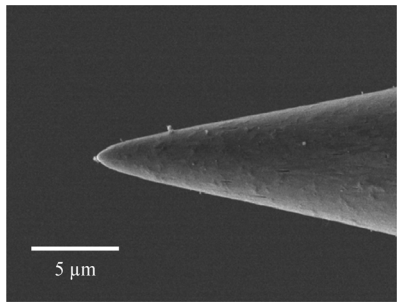

Fig. 1. Scanning electron micrograph of a typical probe tip fabricated by an electro-chemical etching method. The tip size can be controlled by the etching condition.

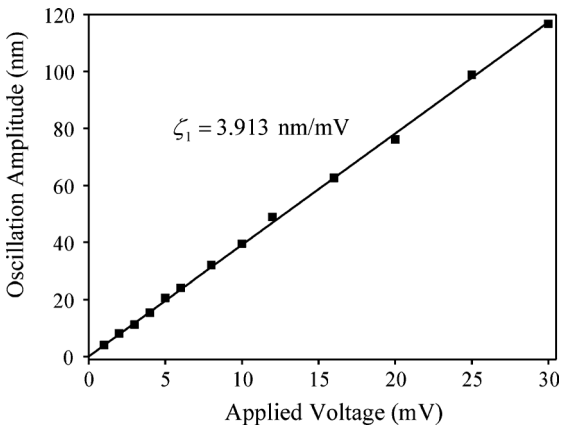

Fig. 2. Measured oscillation amplitude of the quartz tuning fork.

conducting and insulating substrates. The AFM tip was fabricated by an electro-chemical etching method [28] and glued to a quartz tuning fork. Fig. 1 shows the scanning electron micrograph of a tungsten probe tip.

In the THz s-SNOM system, the AFM tip oscillates at the mechanical resonance frequency Ω of a quartz tuning fork. The tip-sample gap distance is then given by

$$g(t) = g_0 + g_1(V)\cos\Omega t \tag{1}$$

where t denotes the time coordinate for the tip oscillation, and the oscillation amplitude g_1 is a function of the excitation voltage V applied to the tuning fork. When scanning the time delay of the THz TDS system, the scattered field $\mathbf{E}_{\rm sc}$ was measured in the far-field region. Since the near field is a highly nonlinear function of $g\ (t)$, the scattered field can be expressed as

$$\mathbf{E}_{\rm sc}(t) = \mathbf{E}_0 + \sum_{m=1}^{\infty} \mathbf{E}_m \cos(m\Omega t). \tag{2}$$

The large background signal $\mathbf{E}_0$ was suppressed by a lock-in demodulation technique to extract harmonic component $\mathbf{E}_m$ [8]–[13]. For the analysis and measurement of the near-field interaction, a precise regulation of the oscillation amplitude is essential. Fig. 2 shows that the measured oscillation amplitude has a linear dependence on the applied voltage with an electromechanical responsivity of $\zeta_1 = g_1/V = 3.913$ nm/mV.

III. Theory

The schematic of a THz s-SNOM is shown in Fig. 3 where the incident THz pulse $(\mathbf{E}_{\rm in})$ induces dipole moments in both

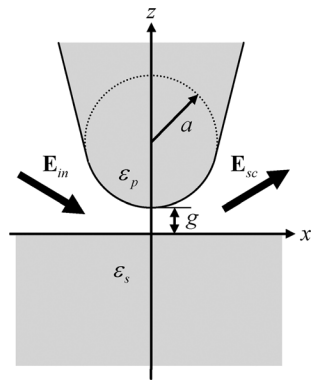

Fig. 3. Schematic diagram of a probe-substrate system in THz s-SNOM. The incident field $\mathbf{E}_{\rm in}$ is p-polarized, and the scattered field $\mathbf{E}_{\rm sc}$ is measured in the far-field region. In the image analysis, the probe is replaced by a polarizable dielectric sphere.

the probe and the substrate, and the probe is strongly coupled with the substrate, generating the scattered THz pulse $(\mathbf{E}_{\rm sc})$. In general, the analytic theory for the near-field interaction in the probe-substrate system is very involved because the electromagnetic boundary conditions should be matched at the surfaces of the probe and the substrate. Moreover, numerical simulations are practically impossible since the metallic probes requires large mesh sizes and the numerical accuracies are usually not good enough for quantitative comparison with experiments.

For an analytic theory of s-SNOMs, the probe tip has usually been replaced by a polarizable sphere of radius a and complex relative permittivity ε_p, as shown in Fig. 3. Because the probe sphere is much smaller than the wavelength of the incident field $\mathbf{E}_{\rm in}$, especially at THz frequencies, quasi-static image methods are applicable to the analysis of the near-field interactions. In the quasi-static image methods, the near-field interaction and the subsequent scattering field $\mathbf{E}_{\rm sc}$ can be calculated by the dipoles induced in the probe and substrate. In the far-field region, the scattering field is given by

$$\mathbf{E}_{\rm sc}(t) = \frac{k^2[\mathbf{r}\times\mathbf{d}(t)]\times\mathbf{r}}{4\pi\varepsilon_0 r^3} \tag{3}$$

where $\mathbf{d}$ is the total induced dipole in the tip-substrate system, $\mathbf{r}$ is the far-field position vector $(r = |\mathbf{r}|)$, k and ε_0 are the wave number and permittivity in vacuum, respectively. In this section we review the point dipole image model and the line dipole image model [21]–[23].

A. Point Dipole Image Method

In the conventional PDIM [8]–[12], the incident field polarizes the probe sphere, resulting in a point image dipole $\mathbf{d}_p^{\rm PD} = \alpha\mathbf{E}_{\rm in}$ at the center of the sphere. The sphere polarizability is given by $\alpha = 4\pi\varepsilon_0 a^3(\varepsilon_p - 1)/(\varepsilon_p + 2)$ where ε_p is the probe permittivity. The probe dipole induces a substrate image dipole, $\mathbf{d}_s^{\rm PD} = \boldsymbol{\beta}_{\rm T}\cdot\mathbf{d}_p^{\rm PD}$ at $z = -h = -(a+g)$. The probe-substrate image generation dyadic is given by $\boldsymbol{\beta}_{\rm T} = \beta(\mathbf{I} - 2\mathbf{u}_x\mathbf{u}_x)$ where $\beta = (\varepsilon_s - 1)/(\varepsilon_s + 1)$, ε_s is the substrate permittivity, $\mathbf{u}_x(\mathbf{u}_z)$ are the unit vectors along the $x(z)$ axes, and $\mathbf{I} = \mathbf{u}_x\mathbf{u}_x + \mathbf{u}_z\mathbf{u}_z$. By taking into account the recursive generation of the point

image dipoles [10], [11], the total image dipole in the probe-substrate system is given by $\mathbf{d}^{\mathrm{PD}} = \boldsymbol{\alpha}^{\mathrm{PD}} \cdot \mathbf{E}_{\mathrm{in}}$ with the effective polarizability tensor

$$\boldsymbol{\alpha}^{\mathrm{PD}} = \frac{\alpha(1-\beta)}{1-\frac{\alpha\beta}{32\pi h^3}}\mathbf{u}_x\mathbf{u}_x + \frac{\alpha(1+\beta)}{1-\frac{\alpha\beta}{16\pi h^3}}\mathbf{u}_z\mathbf{u}_z. \tag{4}$$

In the PDIM, the continuous dipole distributions are usually replaced by point image dipoles. This point-dipole approximation, however, works well only for a large tip-substrate distance. In principle, the electric field from the substrate dipole induces not only a single point dipole but also a continuous dipole distribution in the probe sphere, as we shall see in the LDIM.

B. Line Dipole Image Method

In contrast to the PDIM, the LDIM applies exact electrostatic boundary conditions to all dielectric surfaces of the sphere-substrate system through iteration processes, which results in continuous line image dipole densities. This means that the LDIM is self-consistent within the framework of the polarizable sphere model. Here we describe the LDIM and then present quantitative analyses for the THz near-field interaction in the probe-substrate system [21]–[23].

In the first iteration, the initial dipole moment at the probe sphere is induced by the incident field, resulting in the probe dipole given by

$$\mathbf{d}^{\mathrm{LD}}_{p(1)} = \alpha(1+r)\mathbf{E}_{\mathrm{in}} \tag{5}$$

where we include the reflection coefficient r at the substrate surface because the actual excitation field is the sum of the incident and reflected fields. It should be noted that we have to consider an image dipole of the radiation source for the incident field to match the exact boundary conditions at the substrate surface. The probe dipole in turn induces the substrate image dipole at $z = -h$ given as

$$\mathbf{d}^{\mathrm{LD}}_{s(1)} = \boldsymbol{\beta}_T \cdot \mathbf{d}^{\mathrm{LD}}_{p(1)}. \tag{6}$$

In the second iteration, the substrate point dipole $\mathbf{d}^{\mathrm{LD}}_{s(1)}$ induces a line dipole density $\mathbf{p}^{\mathrm{LD}}_{s(2)}(z,h) = \boldsymbol{\gamma}(z,h,2h) \cdot \mathbf{d}^{\mathrm{LD}}_{s(1)}$. From the exact image theory [21]–[23], we can derive the substrate-probe image generation dyadic defined as

$$\begin{aligned}\boldsymbol{\gamma}(z,h,L) &= \frac{\varepsilon_p - 1}{\varepsilon_p + 1}\left(\frac{a}{L}\right)^3 \delta(z-h+z_K)(\mathbf{I} - 2\mathbf{u}_x\mathbf{u}_x) \\ &\quad + \frac{\varepsilon_p - 1}{(\varepsilon_p+1)^2}\frac{a}{L^2}\left(\frac{h-z}{z_K}\right)^{\frac{1}{\varepsilon_p+1}} \\ &\quad \times [U(z-h+z_K) - U(z-h)][\mathbf{I} + (\varepsilon_p - 1)\mathbf{u}_z\mathbf{u}_z]\end{aligned} \tag{7}$$

where $z_{\mathrm{K}} = a^2/L$ is the Kelvin distance [21], and $\delta(z)$ and $U(z)$ are the Dirac delta and Heaviside unit step functions, respectively.

From the third iteration, we must consider not only the point image dipoles but also the line image dipole densities in both the probe and the substrate. For the nth iteration, the probe ($n \geq 3$) and substrate ($n \geq 2$) dipole densities are given by convolution integrals

$$\begin{aligned}\mathbf{p}^{\mathrm{LD}}_{p(n)}(z,h) &= \int_{-h}^{a-h} dz'\, \boldsymbol{\gamma}(z,h,h-z') \cdot \mathbf{p}^{\mathrm{LD}}_{s(n-1)}(z',h) \\ \mathbf{p}^{\mathrm{LD}}_{s(n)}(z,h) &= \boldsymbol{\beta}_T \cdot \mathbf{p}^{\mathrm{LD}}_{p(n-1)}(-z,h)\end{aligned} \tag{8}$$

and the total dipole moment in the sphere-substrate system is then given by

$$\mathbf{d}^{\mathrm{LD}}(h) = \sum_{n=1}^{\infty}\left[\int_{h-a}^{h} dz\, \mathbf{p}^{\mathrm{LD}}_{p(n)}(z,h) + \int_{-h}^{a-h} dz\, \mathbf{p}^{\mathrm{LD}}_{s(n)}(z,h)\right] \tag{9}$$

where the dipole densities in the first iteration are given by

$$\begin{aligned}\mathbf{p}^{\mathrm{LD}}_{p(1)}(z,h) &= \mathbf{d}^{\mathrm{LD}}_{p(1)}\delta(z-h) \\ \mathbf{p}^{\mathrm{LD}}_{s(1)}(z,h) &= \boldsymbol{\beta}_T \cdot \mathbf{d}^{\mathrm{LD}}_{p(1)}\delta(z+h).\end{aligned} \tag{10}$$

Three-dimensional FEM simulations using a commercial software (HFSS) were in excellent agreement with the LDIM calculations on gold and Si substrates [23].

IV. Analyses, Measurements, and Discussion

The samples for the THz line scan were prepared by evaporating a 35 nm thick gold film on the half surface of a semi-insulating GaAs substrate. The etched tip radius of a tungsten wire was $a \sim 20$ nm. The probe tip was mounted to a quartz tuning fork such that the tip oscillates perpendicularly to the sample surface. As the tip approaches the sample surface, the amplitude, phase, and resonant frequency of the tuning fork's oscillation change. In our experiments, the amplitude was used as a feedback signal for tip-to-sample distance regulation, maintaining a constant tip-substrate distance by controlling the piezo actuator.

The incident THz pulses were p-polarized and focused upon an AFM tip with an incident angle of 60°. The THz scattering signal was detected by a THz photoconductive antenna in the far-field region, and simultaneously the AFM topography of the sample surface was obtained from the feedback signals for the piezo actuators of the nanostages.

A. Line Dipole Image Analysis

The LDIM calculations of the dipole distributions for the gold and GaAs substrates are shown in Fig. 4, where the point dipoles and continuous dipole distribution were discretized into piecewise-constant dipole distributions. The red and blue curves represent calculations for gold and GaAs substrates, respectively. As expected from the standard electrostatic image theory, we can neglect the tangential component (d_x) that is much smaller than the vertical component (d_z). For the LDIM calculation, we used the Drude model for gold and tungsten, where the permittivity is given by

$$\varepsilon(\omega) = 1 - \frac{\omega_p^2}{\omega(\omega + i\omega_\gamma)}. \tag{12}$$

The plasma (damping) frequencies, $\omega_p(\omega_\gamma)$ of gold and tungsten were 2184 THz (1551 THz) and 6.45 THz (14.61 THz), respectively [27]. For the GaAs substrate, we used a frequency-independent permittivity $\varepsilon_s = 12.918$ [26].

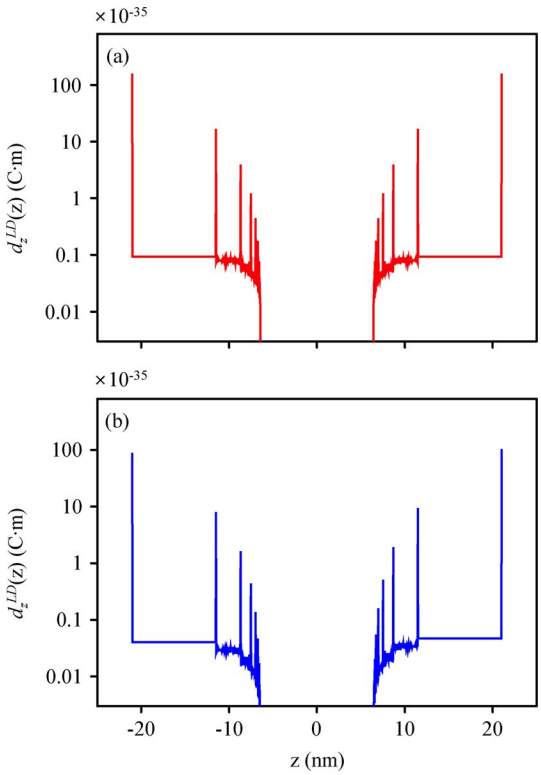

Fig. 4. LDIM calculation of dipole distribution on (a) gold and (b) semi-insulating GaAs substrates. The point dipoles and continuous dipole distribution were discretized into piecewise-constant dipole distributions. The tungsten tip has a radius of $a = 20$ nm. The incident field $\mathbf{E}_{\rm in}$ is p-polarized, and the incident angle is 60°.

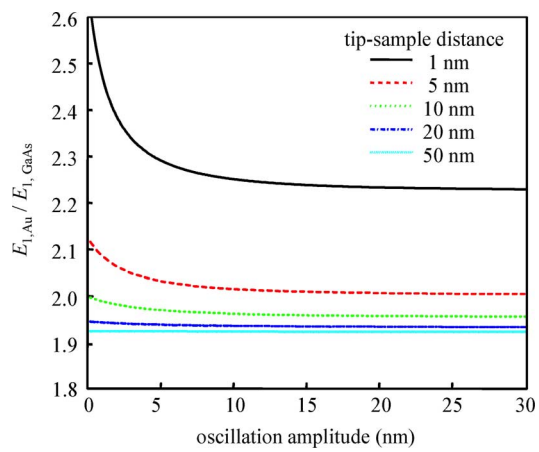

Fig. 5. LDIM calculation of the first harmonic scattering field ratios of gold and GaAs substrates. The tungsten tip has a radius of $a = 20$ nm. The incident field $\mathbf{E}_{\rm in}$ is p-polarized, and the incident angle is 60°.

Fig. 5 shows the LDIM calculations of the first harmonic scattering field ratios for gold and GaAs substrates, $E_{1,\rm Au}/E_{1,\rm GaAs}$. The scattering ratios increase rapidly for small tip-sample distances, and become saturated for large oscillation amplitudes ($g_1 > 15$ nm). This means that the precise control of the tip-substrate distance and oscillation amplitude is crucial for quantitative analysis and measurements. In general, the LDIM calculations result in larger induced dipole moments and also steeper increase of the dipole moments than the PDIM as the tip approaches the substrate. Consequently, the LDIM produces larger harmonic components than the PDIM [23].

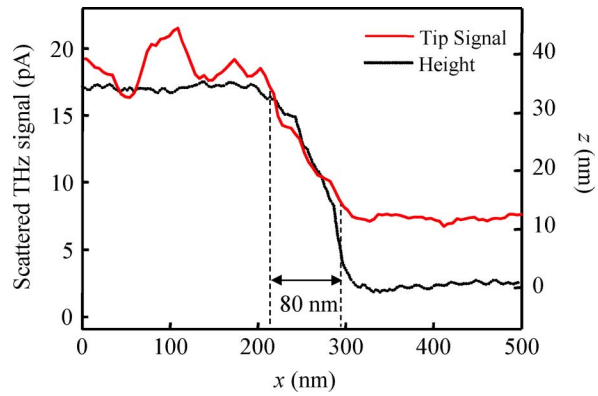

Fig. 6. Line scan across the edge of a gold film on a GaAs substrate. The red and black lines represent the THz scattering signal and the AFM topography, respectively. The 10%-to-90% resolution of the THz s-SNOM was ∼80 nm.

B. THz Line Scan

The THz line scans across the edge of the gold film is shown in Fig. 6, where the first harmonic components (E_1) of the THz scattering signals were used. During the measurements, an oscillation amplitude of $g_1 = 45$ nm was maintained by a proportional-integral-derivative (PID) controller, and the mechanical delay line was fixed at the positive peaks of the THz scattering pulses. The minimum tip-to-sample distance was less than 1 nm, which is the typical operation condition for our AFM system.

The measured tip signal from the Au surface was stronger than that from the GaAs surface as expected from the image theory since the vertical dipole on a metallic surface is enhanced by the image dipole. The THz scattering signal is proportional to the total dipole moment induced in the tip-substrate system, and a metal surface induces larger dipoles than a dielectric surface. The spatial resolution of the THz s-SNOM was ∼80 nm, estimated from the 10%-to-90% transition distance in the line scan. The measured scattering field ratio $(E_{1,\rm Au}/E_{1,\rm GaAs})$ was 2.5 ± 0.3 which is in good agreement with the calculated scattering ratio of ∼2.23, corresponding to the saturation value of scattering ratio for large oscillation amplitude (45 nm) and small tip-sample distance ($\leq$1 nm) used in our measurements.

V. Conclusion

We have used the line dipole image method to analyze the scattering signals in THz pulse s-SNOMs. We have also demonstrated that the THz s-SNOM has a nanoscale resolution of ∼80 nm. The relative ratios of the scattering signals measured on gold and GaAs substrates were in good agreement with calculations by the line dipole image theory. We believe that this is an important step toward quantitative imaging contrast in THz near-field microscopy.

Acknowledgment

The authors wish to thank Dr. H. K. Park at the Hong Kong University of Science and Technology, Dr. J. H. Kim and Dr. Y. H. Han at Samsung Electronics for their contribution to the initial development of the THz near-field microscope.

References

[1] S. Hunsche, M. Koch, I. Brener, and M. C. Nuss, "THz near-field imaging," *Opt. Comm.*, vol. 150, pp. 22–26, 1998.

[2] Q. Chen and X.-C. Zhang, "Semiconductor dynamic aperture for near-field terahertz wave imaging," *IEEE J. Sel. Top. Quantum Electron.*, vol. 7, no. 4, pp. 608–614, Jul./Aug. 2001.
[3] N. C. J. van der Valk and P. C. M. Planken, "Electro-optic detection of subwavelength terahertz spot sizes in the near field of a metal tip," *Appl. Phys. Lett.*, vol. 81, no. 9, pp. 1558–1560, 2002.
[4] T. Yuan, H. Park, J. Xu, H. Han, and X.-C. Zhang, "Field induced THz wave emission with nanometer resolution," *Proc. SPIE*, vol. 5649, pp. 1–8, 2005.
[5] H. T. Chen, R. Kersting, and G. C. Cho, "Terahertz imaging with nanometer resolution," *Appl. Phys. Lett.*, vol. 83, no. 15, pp. 3009–3011, 2003.
[6] H. Park, J. Kim, and H. Han, "THz pulse near-field microscope with nanometer resolution," presented at the 35th Workshop: Physics and Technology of THz Photonics 2005, Erice, Italy, Jul. 20–26, 2005.
[7] H. Park, J. Kim, M. Kim, H. Han, and I. Park, "Terahertz near-field microscope," presented at the Joint 31st International Conference on Infrared Millimeter Waves and 14th International Conference on Terahertz Electronics (IRMMW-THz 2006), Shanghai, China, Sep. 18–22, 2006.
[8] H.-G. von Ribbeck, M. Brehm, D. W. van der Weide, S. Winnerl, O. Drachenko, M. Helm, and F. Keilmann, "Spectroscopic THz near-field microscope," *Opt. Exp.*, vol. 16, no. 5, pp. 3430–3438, 2008.
[9] A. J. Huber, F. Keilmann, J. Wittborn, J. Aizpurua, and R. Hillenbrand, "Terahertz near-field nanoscopy of mobile carriers in single semiconductor nanodevices," *Nano. Lett.*, vol. 8, no. 11, pp. 3766–3770, 2008.
[10] B. Knoll and F. Keilmann, "Enhanced dielectric contrast in scattering-type scanning near-field optical microscopy," *Opt. Commun.*, vol. 182, pp. 321–328, 2000.
[11] R. Hillenbrand and F. Keilmann, "Complex optical constants on a subwavelength scale," *Phys. Rev. Lett.*, vol. 85, no. 14, pp. 3029–3032, 2000.
[12] T. Taubner, R. Hillenbrand, and F. Keilmann, "Nanoscale polymer recognition by spectral signature in scattered infrered near-field microscopy," *Appl. Phys. Lett.*, vol. 85, no. 21, pp. 5064–5066, 2004.
[13] M. Labardi, S. Patanè, and M. Allegrini, "Artifact-free near-field optical imaging by apertureless microscopy," *Appl. Phys. Lett.*, vol. 77, no. 5, pp. 621–623, 2000.
[14] L. Novotny, R. X. Bian, and X. S. Xie, "Theory of nanometric optical tweezers," *Phys. Rev. Lett.*, vol. 79, no. 4, pp. 645–648, 1997.
[15] P. K. Aravind and H. Metiu, "The effects of the interaction between resonances in the electromagnetic response of a sphere-plane structure; Applications to surface enhanced spectroscopy," *Surf. Sci.*, vol. 124, pp. 506–528, 1983.
[16] S. V. Suknov, "Role of multipole moment of the probe in apertureless near-field optical microscopy," *Ultramicroscopy*, vol. 101, pp. 111–122, 2004.
[17] J. A. Porto, P. Johansson, S. P. Apell, and T. López-Ríos, "Resonance shift effects in apertureless scanning near-field optical microscopy," *Phys. Rev. B*, vol. 67, p. 085409.
[18] A. Cvitkovic, N. Ocelic, and R. Hillenbrand, "Analytical model for quantitative prediction of material contrast in scattering-type near-field optical microscopy," *Opt. Exp.*, vol. 15, no. 14, pp. 8550–8565, 2007.
[19] R. Esteban, R. Vogelgesang, and K. Kern, "Tip-substrate interaction in optical near-field microscopy," *Phys. Rev. B*, vol. 75, p. 195410.
[20] M. Brehm, A. Schliesser, F. Čajko, I. Tsukerman, and F. Keilmann, "Antenna-mediated back-scattering efficiency in infrared near-field microscopy," *Opt. Exp.*, vol. 16, no. 15, pp. 11203–11215, 2008.
[21] I. V. Lindell, J. C.-E. Sten, and K. I. Nikoskinen, "Electrostatic image method for the interaction of two dielectric spheres," *Radio. Sci.*, vol. 28, no. 3, pp. 319–329, 1993.
[22] K. Moon, J. Kim, Y. Han, H. Park, E. Jung, and H. Han, "Iterative image method for apertureless THz near-field microscope," presented at the IRMMW-THz 2008, Caltech, California, Sep. 15–19, 2008.
[23] K. Moon, E. Jung, M. Lim, Y. Do, and H. Han, "Quantitative analysis and measurements of near-field interactions in terahertz microscopes," *Opt. Exp.*, vol. 19, no. 12, pp. 11539–11544, 2011.
[24] M. van Exter, Ch. Fattinger, and D. Grischkowsky, "Terahertz time-domain spectroscopy of water vapor," *Opt. Lett.*, vol. 34, no. 20, pp. 1128–1130, 1989.
[25] M. van Exter, Ch. Fattinger, and D. Grischkowsky, "High-brightness terahertz beams characterized with an ultrafast detector," *Appl. Phys. Lett.*, vol. 55, no. 4, pp. 337–339, 1989.
[26] D. Grischkowsky, S. Keiding, M. van Exter, and Ch. Fattinger, "Far-infrared time-domain spectroscopy with terahertz beams of dielectrics and semiconductors," *J. Opt. Soc. Amer. B*, vol. 7, no. 10, pp. 2006–2015, 1990.
[27] M. A. Ordal, R. J. Bell, R. W. Alexander, Jr., L. L. Long, and M. R. Querry, "Optical properties of fourteen metals in the infrared and far infrared: Al, Co, Cu, Au, Fe, Pb, Mo, Ni, Pd, Pt, Ag, Ti, V, and W," *Appl. Opt.*, vol. 24, no. 24, pp. 4493–4499, 1985.
[28] M. Kulawik, M. Nowicki, G. Thielsch, L. Cramer, H.-P. Rust, H.-J. Freund, T. P. Pearl, and P. S. Weiss, "A double lamellae dropoff etching procedure for tungsten tips attached to tuning fork atomic force microscopy/scanning tunneling microscopy sensors," *Rev. Sci. Instrum.*, vol. 74, no. 2, pp. 1027–1030, 2003.

Kiwon Moon received the B.S. and M.S. degrees in electrical engineering from the Pohang University of Science and Technology (POSTECH), Pohang, Korea, in 1998 and 2000, respectively, where he is currently working toward the Ph.D. degree in electrical engineering.

He worked for Samsung Electro-Mechanics form 2000 to 2005, specialized in the design and the epitaxial growth of visible laser diodes and blue light emitting diodes. His main research interests are in spectroscopic terahertz near field microscope, real time terahertz imaging using the asynchronous optical sampling technique, and terahertz devices.

Euna Jung received the B.S. degrees in electrical engineering and chemical engineering, and M.S. and Ph.D. degrees in electrical engineering from the Pohang University of Science and Technology (POSTECH), Pohang, Korea, in 2003, 2005 and 2011, respectively.

She is currently working as a Postdoctoral Fellow at the Center for Information Material. Her main research interests include terahertz biomolecular spectroscopy and medical imaging.

Meehyun Lim received the B.S. degree in electronics and electrical engineering from Chung-Ang University, Seoul, Korea, in 2007, and the M.S. degree in electrical engineering from the Pohang University of Science and Technology (POSTECH), Pohang, Korea, in 2009, where she is currently working toward the Ph.D. degree in electrical engineering.

Her current research interests include terahertz spectroscopy, terahertz devices, and nano electronics.

Youngwoong Do received the B.S. degree in electronics engineering from Kyungpook National University, Daegu, Korea, in 2009, and the M.S. degree in electrical engineering from the Pohang University of Science and Technology (POSTECH), Pohang, Korea, in 2011, where he is currently working toward the Ph.D. degree.

His current research interests include nanophotonics and THz near-field spectroscopy.

Haewook Han (S'92–M'95) received the B.S. and M.S. degrees in electrical engineering from Seoul National University, Seoul, Korea in 1986 and 1988, respectively, and the Ph.D. degree in electrical engineering from the Univerisity of Illinois at Urbana-Champaign, Urbana in 1995. He studied low-threshold GaAs–AlGaAs quantum-well, InGaAs–GaAs–AlGaAs strained quantum-well heterostructure lasers, monolithic integrable semiconductor ring lasers, and two-dimensional photonic crystal semiconductor lasers.

At Bell Laboratories, Murray Hill (1995–1997), he contributed to the development of 980-nm CW room-temperature high-power semiconductor pump lasers grown by metalorgainic chemical vapor deposition (MOCVD). In 1997, he joined the faculty of the Department of Electrical Engineering at the Pohang University of Science and Technology (POSTECH). He invented the first THz plastic photonic crystal fibers in 2001, and demonstrated the single-mode THz pulse transmission. His current research intersests are in the field of high-precision THz time-domain spectroscopy of biomolecules and quantum matters, THz photonic crystal fibers, THz materials and devices, and THz near-field microscopes.

Prof. Han cofounded the Korea THz Forum and served as the Directors of the Center for THz Photonics (1998–2000) and the National Laboratory for Nano-THz Photonics (2005–2009) funded by the Korean Ministry of Science and Technology.